Journal of Magnetic Resonance **140,** 189–199 (1999)
Article ID jmre.1999.1818, available online at http://www.idealibrary.com on IDEAL®

Quantitative Measurement of Longitudinal and Transverse Cross-Relaxation Rates: An Application to the Analysis of the Internal Dynamics of Ranalexin in Water and Trifluoroethanol

T. E. Malliavin,* H. Desvaux,† A. Aumelas,* A. Chavanieu,* and M. A. Delsuc*

**Centre de Biochimie Structurale, INSERM U 414, CNRS UMR C9955, Faculté de Pharmacie, Université de Montpellier I, 15, av. Ch. Flahault, F-34060 Montpellier Cedex 2, France; and †Laboratoire Commun de RMN, Service de Chimie Moléculaire, CEA Saclay, F-91191 Gif sur Yvette Cedex, France*

Received January 22, 1999; revised May 17, 1999

We describe a quantitative processing method which gives access to the longitudinal and transverse cross-relaxation rates from off-resonance ROESY intensities. This method takes advantage of the dependence of the off-resonance ROESY experiments at any mixing time and any spin-lock angle θ on two relaxation matrices, the longitudinal and the transverse ones. This allows one to take into account multistep magnetization transfers even if the measurements are performed only at one or two mixing times. The ratio of the longitudinal to transverse cross-relaxation rates can then be used as a local indicator of the internal dynamics, without assuming a structure or a model of motion. After validation of this processing method by numerical simulations, it is applied to the analysis of the dynamics of the peptide ranalexin dissolved in pure water and in water/TFE.

Key Words: **internal dynamics; off-resonance ROESY; ranalexin; relaxation; spin diffusion.**

1. INTRODUCTION

Determination of molecular structures by NMR is essentially based on the measurement of dipolar cross-relaxation rates between protons, which allows the estimation of the internuclear distances (*1*). The accuracy of the solution structures strongly depends on the accuracy of the distance estimations (*2*), which is mainly limited by two different reasons. First, the NOE intensity between two spins I^i and I^j depends not only on the mutual cross-relaxation, but also on the self-relaxation of each spin and on the cross-relaxation between the spin I^i (I^j) and the other spins through spin diffusion. Second, the cross-relaxation rate is function of the internuclear distance as well as of the dynamics of the interproton vector. This last point makes the structure characterization of flexible molecules difficult. We present below a processing method which solves these two difficulties simultaneously without assuming a motion model, an initial set of distances, or the absence of spin diffusion.

Three kinds of methods exist for the processing of NOE intensities. (i) The most widely used is to estimate lower and upper distance bounds from the intensities. Although this approach is robust, it does not provide quantitative estimates of the relaxation rates. By using pulse sequences designed to remove spin diffusion (*3, 4*), the distance intervals are reduced, but the number of observable cross-peaks and then the amount of experimental information decrease. (ii) The matrix of longitudinal relaxation rates can be derived from the matrix of measured intensities (*5–10*). The efficiency of these methods depends on the number of missing elements in the intensity matrices (due to peak overlap, noise, or artifacts) and on the choice of a motion model and initial distances. (iii) The longitudinal cross-relaxation rates can also be determined without assuming a motional model by the quantitative analysis of each buildup curve using a multiexponential function (*11*), or using a polynomial interpolation of the Taylor development of intensities (*12*). The precision on the relaxation rates is then limited by the accuracy of the intensity measurements and not by the number of missing elements in the intensity matrices. The approach presented here belongs to this last kind of methods: the cross-relaxation rates between two protons are determined by the analysis of the variation of the corresponding cross-peak intensities acquired in different conditions.

A solution suggested to overcome the simultaneous dependence of the cross-relaxation rate on the internuclear distance and on the local dynamics consists of measuring the longitudinal R_{ij} and transverse P_{ij} cross-relaxation rates between I^i and I^j (*13–15*), as these two rates present different dependences on the internal motion. The transverse cross-relaxation rate P_{ij}, which should in principle be monitored by the on-resonance ROESY experiment (*16, 17*), is experimentally inaccessible (*18*). But the off-resonance ROESY experiment allows one to indirectly determine R_{ij} and P_{ij} (*19–21*). This experiment is designed to monitor the relaxation of the spin component I^i_Z aligned with the effective field in the rotating frame obtained by applying an RF irradiation of amplitude ω_1 at an offset Δ. The effective field makes an angle $\theta = \arctan(\omega_1/\Delta)$ with the static magnetic field. In well-defined experimental conditions (*22*), the off-resonance ROESY experiment is free of distortions due to Hartmann–Hahn coherence transfers; it is also unaffected by the offset effects due to

1090-7807/99 $30.00

the angular dispersion between the effective and the static magnetic field directions, which results from the spread of proton resonance frequencies. The associated relaxation matrix Q^θ is related to the longitudinal R and transverse P matrices:

$$Q^\theta = R\cos^2\theta + P\sin^2\theta. \quad [1]$$

Usually the study of internal dynamics of biomolecules through off-resonance ROESY is performed by measuring initial slopes of the buildup curves (see, for instance, Refs. *23–25*) or by calculating iteratively the relaxation matrices Q^θ from the intensity matrices (*26*). However, the measurement of initial slope does not take into account magnetization transfers induced by spin diffusion. On the other hand, the iterative calculation of the relaxation matrix requires the choice of a motion model and of an initial structure. Moreover these two methods do not completely make use of the relations between the buildup curves at various angles θ, since the processing is performed in two separate steps, first along τ_m, then, along θ (see Ref. *27* for a review). In the present work, we propose to simultaneously analyze the off-resonance ROESY intensities as a function of several θ values and few (one or two) mixing times. This approach allows a model-free determination of longitudinal and transverse cross-relaxation rates, while taking spin diffusion into account. The method is validated on simulated data and is shown to be robust even on a partially structured peptide of 20 amino acids, which consequently exhibits a large distribution of internal motion timescales.

2. RESULTS AND DISCUSSION

2.1. Evaluation of Internal Mobility

In the case of homonuclear dipolar relaxation, the longitudinal and transverse cross-relaxation rates between I^i and I^j are

$$R_{ij} = -\tfrac{1}{3}J_{ij}(0) + 2J_{ij}(2\omega_0) \quad [2]$$

$$P_{ij} = \tfrac{2}{3}J_{ij}(0) + J_{ij}(\omega_0), \quad [3]$$

where J_{ij} is the dipolar spectral density function of the proton pair (I^i, I^j) and ω_0 is the proton Larmor frequency (*28*). In our notation, J_{ij} is function of the distance variation as well as of the angular mobility of the vector connecting the two protons.

For large molecules ($\omega_0\tau_c > 1$), longitudinal and transverse cross-relaxation rates have opposite signs (Eqs. [2] and [3]); there is thus a unique value of the angle θ, denoted as θ_0^{ij}, for which the off-resonance ROESY cross-relaxation rate Q_{ij}^θ vanishes. According to Eq. [1], θ_0^{ij} is related to the ratio between the longitudinal and transverse cross-relaxation rates:

$$\frac{R_{ij}}{P_{ij}} = \frac{-J_{ij}(0) + 6J_{ij}(2\omega_0)}{2J_{ij}(0) + 3J_{ij}(\omega_0)} = -\tan^2\theta_0^{ij}. \quad [4]$$

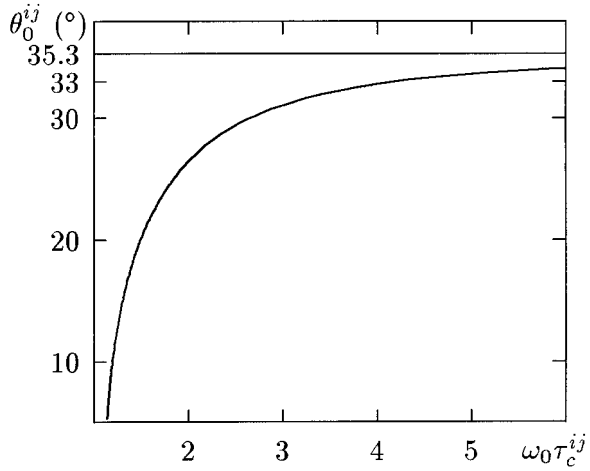

FIG. 1. Variation of θ_0^{ij} as a function of $\omega_0\tau_c^{ij}$ where τ_c^{ij} is the local correlation time.

The absolute value of this ratio is always smaller than 0.5, and θ_0^{ij} is consequently smaller than 35.3°. An examination of Eq. [4] reveals that θ_0^{ij} is an increasing function of the local correlation time τ_c^{ij} as defined in the model of Ref. *29* (Fig. 1). For motions of proton pairs with a correlation time τ_c^{ij} such that $\omega_0\tau_c^{ij} > 5$, the term $J_{ij}(0)$ prevails and θ_0^{ij} is very close to 35.3°.

A qualitative examination of Eq. [4] shows that, whatever the motion model, θ_0^{ij} is a decreasing function of the internal mobility. Let us express $\tan^2\theta_0^{ij}$ as

$$\tan^2\theta_0^{ij} = \frac{1 - 6\zeta_2^{ij}}{2 + 3\zeta_1^{ij}}, \quad [5]$$

where ζ_1^{ij} and ζ_2^{ij} are positive parameters defined as

$$\zeta_1^{ij} = \frac{J_{ij}(\omega_0)}{J_{ij}(0)} \quad [6]$$

$$\zeta_2^{ij} = \frac{J_{ij}(2\omega_0)}{J_{ij}(0)}. \quad [7]$$

An increase of ζ_1^{ij} or ζ_2^{ij} leads to a decrease of θ_0^{ij} (Eq. [5]). Reciprocally, for a given θ_0^{ij} value, ζ_1^{ij} and ζ_2^{ij} are linearly related, and all the lines obtained for different θ_0^{ij} values intersect at one point (Fig. 2). A decrease of θ_0^{ij} leads to an increase of the absolute value of the line slope, and the line undergoes a clockwise rotation. This implies an increase of ζ_1^{ij} or ζ_2^{ij}, which corresponds to an increase of $J_{ij}(\omega_0)$ and/or of $J_{ij}(2\omega_0)$, and finally to an increase of internal mobility.

A direct characterization of the relative mobility of the proton pairs is thus provided by θ_0^{ij}. The simplest idea for determining θ_0^{ij} consists of noting that, in a good approximation, if the cross-relaxation rate $Q_{ij}^{\theta_0^{ij}}$ vanishes then the associ-

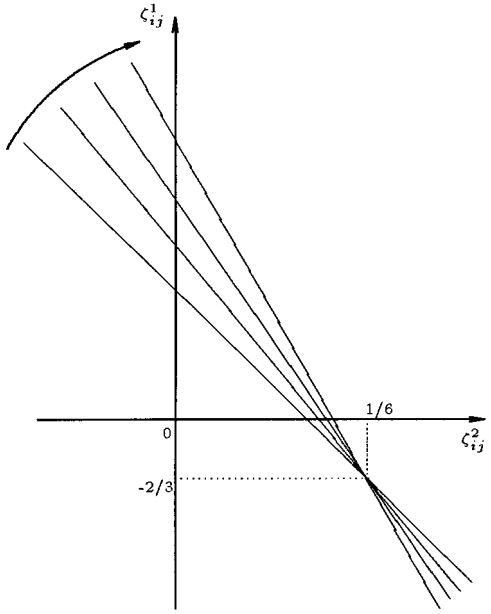

FIG. 2. Representation of ζ_{ij}^1 and ζ_{ij}^2 for different θ_0^{ij}. The physically accessible range of $(\zeta_1^{ij}, \zeta_2^{ij})$ is located in the upper right quadrant of the plane. ζ_1^{ij} and ζ_2^{ij} are linearly related through $\tan^2\theta_0^{ij}$ (Eq. [5]). The corresponding line has a negative slope of $-2/(\tan^2\theta_0^{ij})$ and crosses the ζ_1^{ij} and ζ_2^{ij} axes at positive values of $(1 - 2\tan^2\theta_0^{ij})/(3\tan^2\theta_0^{ij})$ and $\frac{1}{6}(1 - 2\tan^2\theta_0^{ij})$. The different lines obtained for different values of $\tan^2\theta_0^{ij}$ form a bundle, and they all cross at the same point ($\zeta_2^{ij} = \frac{1}{6}$, $\zeta_1^{ij} = -\frac{2}{3}$). For decreasing values of θ_0^{ij}, the line undergoes the rotation shown by the arrow.

ated cross-peak intensity does for short mixing time. The θ_0^{ij} value can thus be determined as the angle θ for which the intensity cancels out. This simple solution is, however, not always suitable. Indeed, the multistep transfers are strongly affected by the choice of the angle θ since the magnitude and the sign of the cross-relaxation rates Q_{ij}^{θ} and the magnitude of the self-relaxation rate Q_{ii}^{θ} change with θ (*27*). As a consequence, the intensity of the spin-diffusion cross-peaks often almost vanishes for a range of θ larger than 10°: an example of such an effect can be seen in Fig. 3. Moreover, when large internal mobility is present ($\omega_0\tau_c^{ij} < 1$), R_{ij} and P_{ij} have the same sign, and θ_0^{ij} is not defined (Eq. [4]), although the dynamic information is still contained in the ratio R_{ij}/P_{ij}. Finally, if the correlation times of the proton pairs surrounding the studied ones are very different, due to multistep transfers for nonvanishingly small mixing time, the angle for which the cross-peak vanishes is not necessarily equal to θ_0^{ij}. We consequently suggest first to determine the cross-relaxation rates P_{ij} and R_{ij} and then to calculate θ_0^{ij} from their ratio.

2.2. Determination of the Longitudinal and Transverse Cross-Relaxation Rates

The peak intensities measured by off-resonance ROESY at a given angle θ and a mixing time τ_m can be expressed as an intensity matrix $\mathcal{I}(\theta, \tau_m)$ (*30, 31*):

$$\mathcal{I}(\theta, \tau_m) = \exp(-Q^{\theta}\tau_m)\mathcal{I}_0, \quad [8]$$

where $\mathcal{I}_0$ is the intensity diagonal matrix for a vanishingly small mixing time. It will be taken equal to **1** in the following. The development at the order p along τ_m of the off-resonance ROESY cross-peak intensity between I^i and I^j can be written as (for $i \neq j$)

$$\mathcal{I}_{ij}(\theta, \tau_m) \cong -Q_{ij}^{\theta}\tau_m I_0 + [(Q^{\theta})^2]_{ij}\frac{\tau_m^2}{2} - \cdots + [(Q^{\theta})^p]_{ij}\frac{(-1)^p\tau_m^p}{p!}. \quad [9]$$

Using the expression of matrix Q^{θ} (Eq. [1]), Eq. [9] becomes

$$\mathcal{I}_{ij}(\theta, \tau_m) \cong \sum_{q=1}^{p}\frac{(-1)^q\tau_m^q}{q!}\sum_{s=0}^{q}(\cos^2\theta)^s(\sin^2\theta)^{(q-s)} \times [T_q^{q-s}(R, P)]_{ij}, \quad [10]$$

where $[T_q^{q-s}(R, P)]_{ij}$ is the (i, j) element of the matrix $[T_q^{q-s}(R, P)]$, which is a polynomial of matrices R and P. The polynomial degree is s in R and $q - s$ in P. The list of $T_q^{q-s}(R, P)$ matrices is given in Table 1 for $q = 1$, $q = 2$, and $q = 3$.

Considering the particular cross-peak between I^i and I^j, Eq. [10] defines a linear relation between the vector $\mathcal{I}_{ij}$ composed of all intensity values measured at different mixing times τ_m and angles θ, and the vector $\mathcal{T}_{ij}$ composed of the (i, j) elements of the $T_q^{q-s}(R, P)$ matrices. Among all these elements, our principal interest will be in the cross-relaxation rates $R_{ij} = [T_1^1(R, P)]_{ij}$ and $P_{ij} = [T_1^0(R, P)]_{ij}$. Indeed, exploitation of the other coefficients requires the knowledge of almost all elements which is experimentally prevented by noise and peak overlaps. Equation [10] can be expressed analytically as a polynomial of order p in $\cos^2\theta$:

$$\mathcal{I}_{ij}(\theta, \tau_m) \cong \sum_{q=0}^{p}G_q^{ij}(\tau_m)(\cos^2\theta)^q, \quad [11]$$

the coefficients $G_q^{ij}(\tau_m)$ being polynomials in τ_m of order p. Only the polynomials $G_0^{ij}(\tau_m)$ and $G_1^{ij}(\tau_m)$ depend directly on R_{ij} and P_{ij}.

$$G_0^{ij}(\tau_m) = -P_{ij}\tau_m + \alpha_{02}^{ij}\tau_m^2 + \cdots + \alpha_{0p}^{ij}\tau_m^p \quad [12]$$

$$G_1^{ij}(\tau_m) = -(R_{ij} - P_{ij})\tau_m + \alpha_{12}^{ij}\tau_m^2 + \cdots + \alpha_{1p}^{ij}\tau_m^p, \quad [13]$$

where α_{uv}^{ij} are (i, j) elements of matrices polynomials in R and P. If the processing is performed in two steps along θ and τ_m separately, $n \geq p + 1$ angles θ are required to determine $G_0^{ij}(\tau_m)$ and $G_1^{ij}(\tau_m)$, and $n \geq p$ mixing times are then required

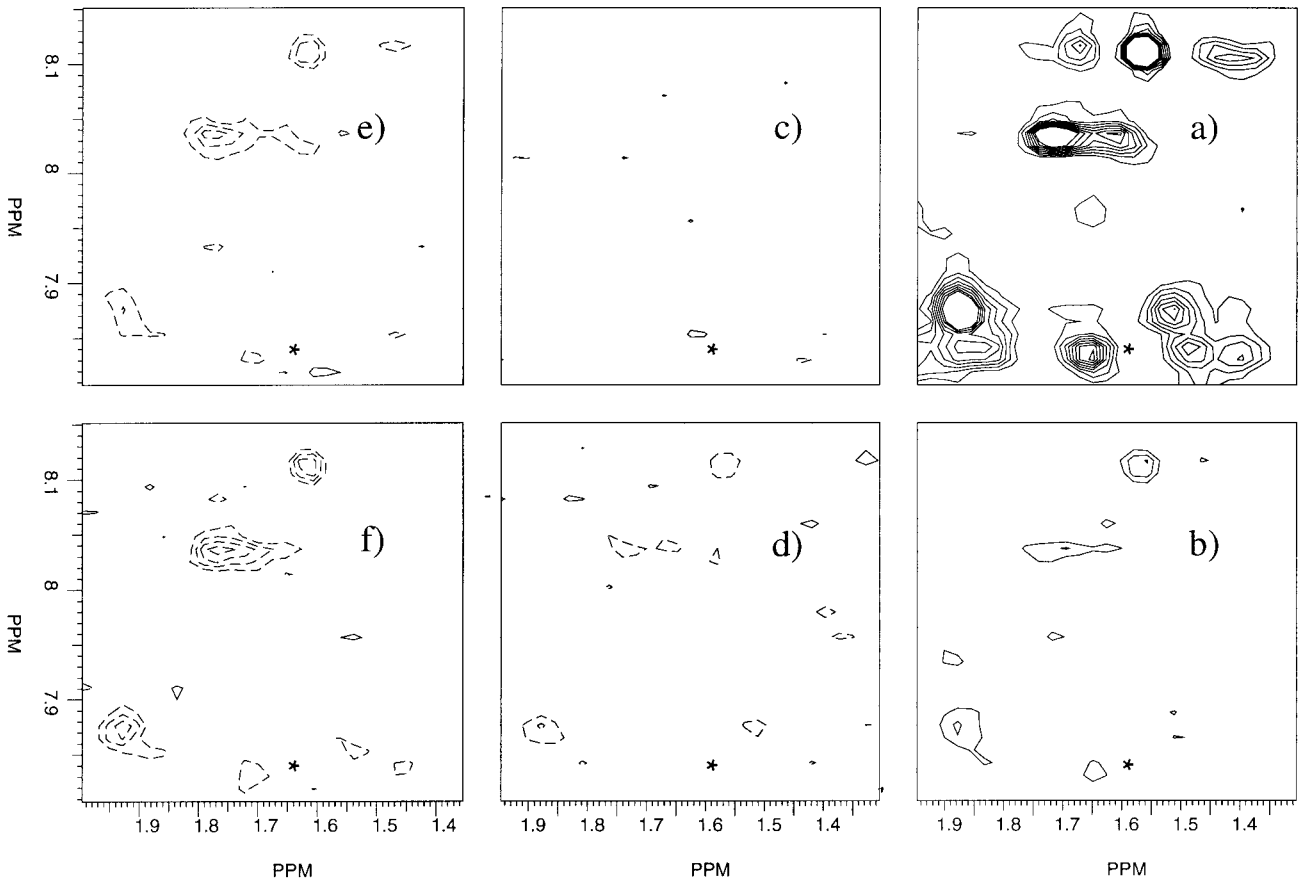

FIG. 3. Subspectra of the HN–Hα region of off-resonance ROESY acquired on ranalexin in 30% TFE at θ angles of 5° (a), 30° (b), 35° (c), 40° (d), 45° (e), and 55° (f). All spectra are plotted at the same level. The cross-peak between HN and Hβ of lysine 19, which cancels out for a large interval of θ values, is indicated by a star. The positive contours (same sign as the diagonal peaks) are drawn with solid lines and the negative contours in dotted lines.

to determine R_{ij} and P_{ij}. Thus a total number of $p(p + 1)$ measurements are needed. But, since the $G_q^{ij}(\tau_m)$ polynomials are related through Eq. [10], working simultaneously along θ and τ_m allows one to reduce the number of measurements to $p(p + 3)/2$, which is the number of $[T_q^{q-s}(R, P)]_{ij}$ elements.

TABLE 1
Expressions of the $T_q^{q-s}(R, P)$ Matrices with s Varying from 0 to q, and q Varying from 1 to 3

q	s	$T_q^{q-s}(R, P)$
1	0	R
1	1	P
2	0	R^2
2	1	$RP + PR$
2	2	P^2
3	0	R^3
3	1	$R^2P + RPR + PR^2$
3	2	$RP^2 + PRP + P^2R$
3	3	P^3

As instance for $p = 2$ (respectively, $p = 3$), the number of $[T_q^{q-s}(R, P)]_{ij}$ elements is 5 (resp., 9), while $p(p + 1) = 6$ (resp., *12*). Moreover the simultaneous processing of all $\mathcal{J}_{ij}(\theta, \tau_m)$ values takes advantage of particular properties of relaxation to improve the accuracy of the determination of the cross-relaxation rates. Indeed the development of Eq. [9] at a given order p is more valid: (i) for large θ, since the self-relaxation is more efficient (transverse relaxation is known to be less sensitive to spin diffusion than the longitudinal one), and (ii) for θ close to θ_0^{ij}, since the cross-relaxation is less efficient. To profit from these remarks, it seems reasonable to deal with a set of experiments (τ_m, θ) such that the number n of different angles θ is at its largest.

The processing of off-resonance ROESY intensities has been performed up to now (*15*) using a first-order development of Eq. [10] ($p = 1$). *A priori* the larger p is, the better multistep transfers are taken into account. However, if we consider the third-order development, the $\mathcal{J}_{ij}(\theta, \tau_m)$ depends on nine parameters, and at least three mixing times are required (see above). Considering only three τ_m values leads to unstable

numerical procedure in the presence of noise. This case will consequently not be discussed further, and we here consider the second-order development ($p = 2$):

$$\mathcal{I}_{ij}(\theta, \tau_m) \cong -\tau_m \cos^2\theta R_{ij} - \tau_m \sin^2\theta P_{ij} + \frac{\tau_m^2}{2}\cos^4\theta [R^2]_{ij} + \frac{\tau_m^2}{2}\cos^2\theta \sin^2\theta [RP + PR]_{ij} + \frac{\tau_m^2}{2}\sin^4\theta [P^2]_{ij}. \quad [14]$$

For each cross-peak, the complete set of intensities measured at all the mixing times τ_{m_l} and θ_k values considered, the corresponding Eq. [14] can be put together to form

$$\mathcal{I}_{ij} = \mathcal{A}\mathcal{T}_{ij}, \quad [15]$$

where $\mathcal{I}_{ij}$ is a set of intensity measured at several θ (θ_k, $1 \le k \le n$) and mixing times (τ_{m_l}, $1 \le l \le m$) values, and $\mathcal{T}_{ij}$ is

$$\mathcal{T}_{ij} = (R_{ij}, P_{ij}, [R^2]_{ij}, [RP + PR]_{ij}, [P^2]_{ij}). \quad [16]$$

The matrix $\mathcal{A}$ is a (nm, 5) matrix in which each row is

$$\left(-\tau_{m_l}\cos^2\theta_k, \quad -\tau_{m_l}\sin^2\theta_k, \quad \frac{\tau_{m_l}^2}{2}\cos^4\theta_k, \quad \frac{\tau_{m_l}^2}{2}\cos^2\theta_k \sin^2\theta_k, \quad \frac{\tau_{m_l}^2}{2}\sin^4\theta_k \right), \quad [17]$$

l varying from 1 to m and k from 1 to n.

If the intensities have been measured at two mixing times τ_{m_1} and τ_{m_2}, the rank of the matrix $\mathcal{A}$ is 5, and Eq. [15] can be solved by a linear least-squares fitting method.

If the intensities have been measured only at one mixing time τ_m, it is no longer possible to invert Eq. [15]. There is, however, an empirical way to take into account a second-order development in τ_m. Using trigonometric relations, Eq. [14] can be written as

$$\mathcal{I}_{ij}(\theta, \tau_m) \cong \alpha_0^{ij} + \alpha_1^{ij}\cos^2\theta + \alpha_2^{ij}\cos^4\theta \quad [18]$$

$$\mathcal{I}_{ij}(\theta, \tau_m) \cong \beta_0^{ij} + \beta_1^{ij}\cos(2\theta) + \beta_2^{ij}\cos(4\theta). \quad [19]$$

The α's and β's coefficients can be computed from the set of $\mathcal{I}_{ij}(\theta, \tau_m)$ by using a linear least-squares fitting method. Using Eq. [14], these coefficients can be expressed as a function of $[T_q^{q-s}(R, P)]_{ij}$:

$$\mathcal{C}_{ij} = \mathcal{B}\mathcal{T}_{ij}, \quad [20]$$

TABLE 2
Comparison of the $P_{ij} - R_{ij}$, $P_{ij} + R_{ij}$ (I) and the $[P^2]_{ij} - [R^2]_{ij}$, $[P^2]_{ij} + [R^2]_{ij}$ (II) Pairs

τ_c (ns)	Slope (I)	Correlation coefficient (I)	Slope (II)	Correlation coefficient (II)
1	1.95	0.94	1.37	0.99
2	2.67	0.99	1.41	0.99
3	2.86	1.00	1.41	0.99
4	2.91	1.00	1.41	0.99
5	2.95	1.00	1.42	0.99

Note. The slopes and correlation coefficients obtained by linear regression analysis are given for different values of the overall correlation time τ_c. Internal motions are simulated through local order parameters (see Experimental).

where

$$\mathcal{C}_{ij} = (\alpha_0^{ij}, \alpha_1^{ij}, \alpha_2^{ij}, \beta_0^{ij}, \beta_1^{ij}, \beta_2^{ij}) \quad [21]$$

and

$$\mathcal{B} = \begin{pmatrix} 0 & -\tau_m & 0 & 0.5\tau_m^2 & 0 \\ -\tau_m & \tau_m & 0 & -\tau_m^2 & 0.5\tau_m^2 \\ 0 & 0 & \tau_m^2 & \tau_m^2 & -\tau_m^2 \\ -8\tau_m & -8\tau_m & 3\tau_m^2 & 3\tau_m^2 & 3\tau_m^2 \\ -2\tau_m & 2\tau_m & \tau_m^2 & -\tau_m^2 & 0 \\ 0 & 0 & \tau_m^2 & \tau_m^2 & -2\tau_m^2 \end{pmatrix}. \quad [22]$$

The rank of the matrix $\mathcal{B}$ is 4, whereas the size of the vector $\mathcal{T}_{ij}$ is 5: one needs a supplementary linear equation in order to invert the system of Eq. [20]. The self- and cross-relaxation rates have opposite signs in the matrix R, whereas they have the same signs in the matrix P. Thus, the $[R^2]_{ij}$ terms should be small with respect to the $[P^2]_{ij}$ terms, and the $[P^2]_{ij} - [R^2]_{ij}$ and $[P^2]_{ij} + [R^2]_{ij}$ terms should be of the same order of magnitude. Moreover, as shown by numerical simulations, they are proportional, which provides the fifth linear equation required to solve the system of Eq. [20].

Indeed, the parameters $P_{ij} - R_{ij}$, $P_{ij} + R_{ij}$, $[P^2]_{ij} + [R^2]_{ij}$, and $[P^2]_{ij} - [R^2]_{ij}$ were simulated as described under Experimental, using values from 1 to 5 ns for the overall correlation time τ_c. By linear regression analysis, simulated $[P^2]_{ij} - [R^2]_{ij}$ and $[P^2]_{ij} + [R^2]_{ij}$ are found to be proportional (Table 2). The proportionality coefficient is 1.41 and is very weakly dependent on the local correlation time in the range 0.36–5 ns, since it exhibits a variation inferior to 0.05 (3.6%). In contrast the variation of the coefficient between $P_{ij} - R_{ij}$ and $P_{ij} + R_{ij}$ is 1.0 which represents 40%.

TABLE 3
Test of the Processing Methods on Simulated Intensities

Method	e_{ij}	Number of rates	Slope	Correlation coefficient	ϵ (%)
100–200 ms	0.0	1272	0.98	1.00	1.0
	0.0005	812	0.98	1.00	1.0
	0.001	444	0.99	0.99	11.9
	0.002	178	1.00	0.99	14.0
200–300 ms	0.0	1272	0.95	1.00	2.8
	0.0005	964	0.95	1.00	10.5
	0.001	698	0.96	0.99	14.2
	0.002	344	0.96	0.99	16.2
100–300 ms	0.0	1272	0.97	1.00	1.5
	0.0005	906	0.98	1.00	8.9
	0.001	560	0.98	1.00	10.6
	0.002	250	0.99	0.99	13.0
100 ms	0.0	1272	1.02	1.00	13.3
	0.0005	636	1.02	0.99	20.2
	0.001	284	1.03	0.97	24.9
	0.002	104	1.06	0.95	28.6
200 ms	0.0	1272	1.02	1.00	23.2
	0.0005	906	1.02	0.99	18.4
	0.001	584	1.02	0.99	18.9
	0.002	262	1.03	0.98	22.7
300 ms	0.0	1272	1.01	0.99	30.6
	0.0005	1036	1.01	0.99	22.7
	0.001	782	1.01	0.99	21.0
	0.002	390	1.01	0.99	19.0
100–200 ms	0.0	1272	0.98	1.00	1.3
(8 θ values)	0.0005	820	0.99	1.00	12.0
	0.001	426	0.99	0.99	13.9
	0.002	180	0.99	0.99	17.5
100–200 ms	0.0	1272	0.98	1.00	1.0
(5 θ values)	0.0005	788	0.98	0.99	16.3
	0.001	404	0.98	0.99	19.5
	0.002	158	0.96	0.97	22.2

Note. The mixing time values, the error e_{ij} added to intensities, and the number of simulated cross-peaks kept for regression analysis are given. The calculated and theoretical longitudinal R_{ij} and transverse P_{ij} cross-relaxation rates are compared using linear regression parameters (line slope, correlation coefficient) and using the relative mean error ϵ (Eq. [24]).

2.3. Validation of the Processing Method on Simulated Intensities

Two processing protocols were tested by numerical simulations: the "one-mixing-time" method based on Eqs. [18–22], and the "two-mixing-time" method based on Eqs. [15–17]. Simulated intensity values were calculated at mixing time of 100, 200, and 300 ms and at θ values 5, 10, 15, 20, 25, 30, 35, 40, 45, 50, and 55°. Different sets of τ_m values (100–200 ms, 200–300 ms, 100–300 ms, 100 ms, 200 ms, and 300 ms) and different thermal noises e_{ij} (0.0, 0.0005, 0.001, and 0.002) were used. The set of intensities of each hydrogen pair (i, j) considered was processed independently of the other hydrogen pairs, to extract the (i, j) longitudinal and transverse cross-relaxation rates. Only P_{ij} and R_{ij} values were kept after the processing. Indeed, the $[P^2]_{ij}$, $[R^2]_{ij}$ and $[RP + PR]_{ij}$ terms are used to take into account all the multistep transfers of order larger than 2, resulting in poor correlation between these terms and the corresponding theoretical ones.

For each set of τ_m, the proton pairs included in the analysis corresponded to mean relative error σ_{ij} (Eq. [25]) smaller than 33%. Using linear regression analysis, the slopes, the correlation coefficients, and the relative mean error ϵ (Eq. [24]) between the theoretical and simulated cross-relaxation rates were determined (Table 3). The results obtained for the set of mixing times 100–200 ms are graphically displayed in Fig. 4.

In Table 3, all correlation coefficients between theoretical and extracted cross-relaxation rates are larger than 0.95, and the majority of them are equal to 1.00 or 0.99. The method of processing based on two mixing times slightly underestimates the cross-relaxation rates. If both τ_{m1} and τ_{m2} are larger than 100 ms, the approach induces more biases: the values of regression slopes range between 1.00 and 0.97 for the 100–200 and 100–300 ms sets, whereas they range between 0.96 and 0.95 for the 200–300 ms set. Moreover, the ϵ values are smaller for the 100–200 and 100–300 ms sets than for the 200–300 ms set: as expected, the second-

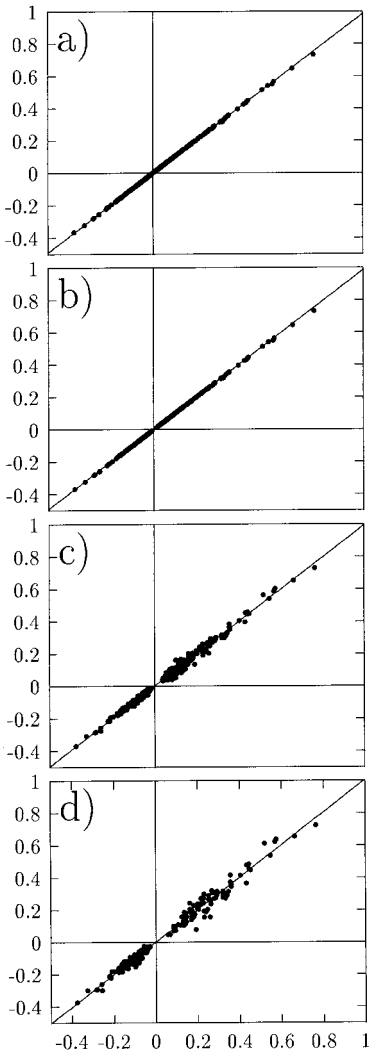

FIG. 4. Results of the two-mixing-time processing method on simulated intensities. The mixing time set is 100–200 ms and the errors e_{ij} are 0.0 (a), 0.0005 (b), 0.001 (c), and 0.002 (d). The computed cross-relaxation rates (Hz, *y* axis) are plotted against the theoretical ones (Hz, *x* axis). The longitudinal cross-relaxation rates R_{ij} are negative; the transverse cross-relaxation rates P_{ij} are positive. The results of linear regression analyzes are shown by continuous straight lines.

order development is more efficient for short than for long mixing times.

For the method using one-mixing-time sets, the regression slopes are larger than 1, leading to overestimated rates. For τ_m equal to 200 or 300 ms, the regression slope values are between 1.01 and 1.03: the bias induced at large τ_m by the second-order approximation is thus reduced for the one-mixing-time set with respect to the 200–300 ms set. On the other hand, for τ_m equal to 100 ms, the regression slope is in the range of 1.02–1.06. Also, the bias induced on the computed rates is larger in the case of τ_m = 100 ms than for τ_m of 200 and 300 ms. This behavior is especially obvious for large errors e_{ij} (0.002). It is probably a consequence of small intensities simulated for short mixing times which become more sensitive to the addition of noise and restrict the number of proton pairs on which the average is computed.

The mean relative errors ϵ of the cross-relaxation rates are smaller for the two-mixing-time sets than for the one-mixing-time sets, which certainly results from the use of the empirical relation between $[R^2]_{ij} - [P^2]_{ij}$ and $[R^2]_{ij} + [P^2]_{ij}$ in the latter case, and from the larger number of input intensities in the first case. The mean relative errors ϵ are smaller than 30%, which correspond to errors of 5% on distances. This increase of precision relative to what is obtained using only NOESY experiments (*32*) probably results from the dependence of the intensities and of the magnetization transfer on the angle θ.

The appropriate number of θ values when using the two-mixing-time method was explored on simulated intensities at 100 at 200 ms. Two sets of 8 θ values (10, 15, 20, 30, 35, 40, 50, and 55°) and 5 θ values: (10, 20, 30, 40, and 50°) were used. The results of simulation are given in Table 3: the linear regression parameters and the number of proton pairs kept for the analysis are similar to those observed using the set of 11 θ values, but the relative mean errors ϵ (Eq. [24]) are significantly larger if noisy intensities are processed. The number *n* of θ values close to 10 thus appears to be a good compromise between reasonable experiment duration and quantitative processing.

The numerical stability of processing methods at 200 ms and 100–200 ms was tested using a Monte Carlo simulation (Table 4). Two proton pairs corresponding to θ_0^{ij} values of 30.6 and 34.9° were used. The Monte Carlo simulation shows that for noise levels σ_{ij} smaller than 15%, the $\langle\theta_0^{ij}\rangle$ value is at most at

TABLE 4
Monte Carlo Simulations Performed on Four Data Sets Corresponding to θ_0^{ij} of 30.6° and 34.9°

Curves	e_{ij}	σ_{ij}	$\langle\theta_0^{ij}\rangle$ (°)	Standard deviation (°)
100–200 ms, θ_0 = 30.6°	0.00005	3.1	30.6	0.3
	0.0001	6.1	30.5	0.8
	0.0002	12.2	30.5	1.5
	0.0005	30.6	30.0	4.3
100–200 ms, θ_0 = 34.9°	0.0002	1.8	35.0	0.2
	0.0005	4.6	34.9	0.5
	0.001	9.2	34.9	1.0
	0.002	18.4	34.8	2.2
200 ms, θ_0 = 30.6°	0.00005	2.3	30.7	0.1
	0.0001	4.6	30.7	0.2
	0.0002	9.2	30.7	0.4
	0.0005	23.0	30.7	1.1
200 ms, θ_0 = 34.9°	0.0002	1.4	34.7	0.1
	0.0005	3.5	34.7	0.3
	0.001	7.0	34.7	0.6
	0.002	14.1	35.0	1.2

Note. The processing methods at 200 ms and 100–200 ms were tested. The noise is expressed as the error (e_{ij}) and as the noise level (σ_{ij}, Eq. [25], expressed in percentages).

0.2° from its theoretical value. For the same noise levels, the standard deviation on θ_0^{ij} in degrees is about one-tenth of σ_{ij} expressed in percentages. The two processing methods are consequently stable. The stability of the one-mixing-time method, which appears to be better because of smaller standard deviations on θ_0^{ij}, may come from the external constraint imposed through the ratio of $[P^2]_{ij} + [R^2]_{ij}$ and $[P^2]_{ij} - [R^2]_{ij}$.

2.4. Experimental Analysis of Ranalexin Mobility

Ranalexin (FLGGLIKIVPAMICAVTKKC) is an antimicrobial peptide extracted from the skin of the American bullfrog *Rana catesbeiana*. The two cysteines, Cys 14 and Cys 20, are linked by a disulfide bridge and form a cycle at the C-terminal part of the peptide. The internal mobility of ranalexin was analyzed in water and 30% trifluoroethanol (TFE) by determining cross-relaxation rates and θ_0^{ij} values. Ninety-four cross-peaks were analyzed for the water sample and 162 for the sample in 30% TFE.

The intensity curves were processed using the one-mixing-time method. The error in degrees on θ_0^{ij} was taken equal to one-tenth of σ_{ij} calculated from the intensity set composed of 11 θ_k. Only the proton pairs for which the error on θ_0^{ij} was smaller than 1° (46 pairs in water and 89 pairs in TFE) were kept for further analysis. The overall precision on θ_0^{ij} was independently determined by comparing θ_0^{ij} values measured on pairs of symmetric cross-peaks or on pairs of cross-peaks correlating one proton to two geminal protons. The mean difference was determined using 24 pairs in 30% TFE and is equal to 0.40°. In water, this value computed on 13 pairs is 0.46°. The mean θ_0^{ij} is 33.3° in 30% TFE and 31.4° in water. If we consider a Lorentzian spectral density function, the corresponding correlation time is 1.2 and 0.8 ns, respectively, values consistent with the peptide size.

The distribution of θ_0^{ij} measured in water and in 30% TFE (Fig. 5) reveals a larger internal mobility if one proton is located in the side chains. In water, the N-terminal part of the peptide is more mobile than in 30% TFE. This observation is consistent with other experimental data available on ranalexin (*33*). Indeed, it was impossible, because of the peptide flexibility, to determine its solution structure in water, whereas in 30% TFE, the structure of the N-terminal part was found to be an α-helix. Furthermore, weak NOE cross-peaks were observed in water between amide protons, and they are located into the 16–20 sequence region, in which large θ_0^{ij} values are observed. The measurements performed here confirm that, in water, the N-terminal part (*1–5*) of the peptide is not structured, whereas the C-terminal part (*6–20*), which contains the cycle, probably has the same structure than that previously observed in 30% TFE.

In the case of large internal mobility ($\omega_0 \tau_l^{ij} < 1.1$), the longitudinal and transverse cross-relaxation rates have the same sign, and θ_0^{ij} is not defined (Eq. [4]). In ranalexin, the proton pairs Hϵ and $NH_3\zeta$ of lysines (Lys 7, 18, and 19 in water and Lys 7 in 30% TFE) present both positive longitudinal and transverse cross-relaxation rates, which certainly results from the superposition of dipolar relaxation and exchange with water.

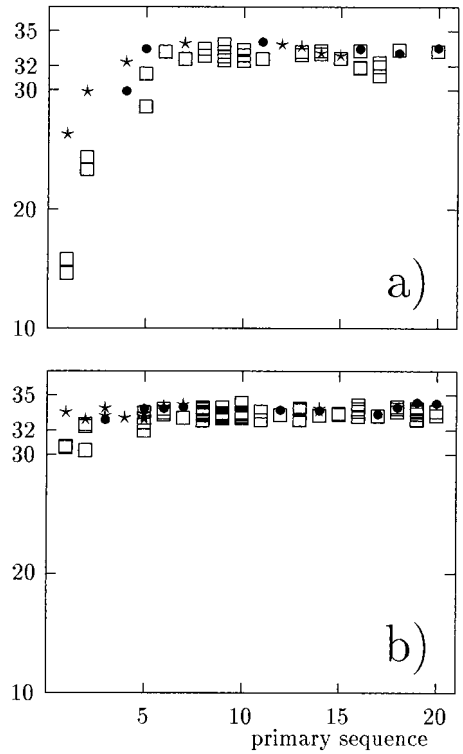

FIG. 5. Experimental θ_0^{ij} values measured on ranalexin in water (a) and in 30% TFE (b). The measurements are plotted with the smallest residue number involved into the analyzed cross-peak. Different kinds of cross-peaks, involving backbone protons of the same residue (●), backbone protons of two different residues (*), or one side chain proton (□), are indicated.

3. CONCLUSION

We have described a processing method which gives access to the longitudinal and transverse cross-relaxation rates from off-resonance ROESY experiment. This approach is based on a second-order development as a function of the mixing time of the relaxation matrix evolution combined to the equation which relates the relaxation matrix at any angle θ to the longitudinal and transverse matrices. The cross-peak intensity at any mixing time and any angle θ then only depends on five parameters, two of which are the desired cross-relaxation rates. Thanks to the exploitation of the simultaneous dependence on θ and τ_m, even using a small number of τ_m (one or two), the method is able to take into account spin-diffusion phenomena for mixing times up to 300 ms. The determination of R_{ij} and P_{ij} exhibits also the advantage of allowing the application of the method to cross-peaks mainly produced by spin diffusion for which the cross-peak intensities almost vanish on a large range of θ preventing

any direct determination of θ_0^{ij} from the intensity curve. The processing is robust with respect to the presence of noise in the data set, since the standard deviation on θ_0^{ij}, computed by Monte Carlo simulation, is smaller than 1° for noise comparable to experimental ones. For simulated intensity sufficiently large with respect to the noise level, the analysis of $\mathcal{J}_{ij}(\theta, \tau_m)$ provides cross-relaxation rates consistent with the theoretical ones for distances between 1.9 and 3.9 Å and motion timescales between 0.36 and 5 ns.

The cross-relaxation rates are obtained in arbitrary units directly from the intensities without assuming a motion model or a structure for the studied molecule. A more detailed analysis of the cross-relaxation rates can be performed in two ways. Assuming a motional model, it is possible to determine a local correlation time and mean distances without internal reference as is done for small molecules (*23*). On the other hand, the θ_0^{ij} parameter can be computed without assumption, and the relative mobility of the interhydrogen vector assessed in a way which becomes independent of the peak integration mask and is then less sensitive to systematic biases. Nevertheless, the variation of θ_0^{ij} with the motion timescale is nonlinear. This puts an upper limit on the motions that can be distinguished; typically $\omega_0\tau_c^{ij}$ should be smaller than about 5. But, the sensitivity of the method is well-adapted to the study of internal dynamics of mobile, partly unfolded, or nascent structures for which the use of chemical shift indexes (*34*) is currently the principal NMR source of information. This was experimentally observed and confirmed on ranalexin peptide since results consistent with other experimental data were obtained. The proposed method has detected the formation of partial 3D structures when the total 3D structure was not determined by classical methods and when the NOE and chemical shifts only indicated conformational equilibrium between several conformations (*33*).

4. EXPERIMENTAL

4.1. Protocol for Numerical Simulations

Theoretical intensities were simulated using the program CROWD (*35*) from the hydrogen coordinates of an NMR conformer of toxin γ (*36*, PDB entry: 1cxn). We have considered 636 proton pairs for which NOESY intensities are larger than 0.005 for a mixing time of 200 ms; the corresponding distances are in the 1.8–3.9 Å range. Local internal mobility was simulated in the frame of a local correlation time model (*29*), which was chosen for the sake of simplicity. In this model, the local correlation time τ_c^{ij} between I^i and I^j is computed as

$$\tau_c^{ij} = S_i S_j \tau_c, \qquad [23]$$

where τ_c is the overall correlation time, and S_i and S_j are correlation time correction factors associated to spins I^i and I^j. The product S_iS_j can be considered as an order parameter of the H–H vector and allows the simulation of the variation of mobility along the structure. The S_i factor was taken equal to 1 for the backbone nuclei, equal to 0.8 for the H^β–H^γ, and equal to 0.6 for the other side chain nuclei. As an example, the smallest scaling coefficient S_iS_j applied to the overall correlation time is 0.36, a value consistent with the experimental order parameters measured on protein side chains (*37, 38*). If not stated otherwise, the value of τ_c was taken equal to 3 ns, and the proton Larmor frequency was 600 MHz. The diagonal terms of the matrix Q^θ were multiplied by 1.25 in order to simulate external relaxation leakages.

The discrepancy between the two sets of cross-relaxation rates X_{ij}^{theo} (used to compute simulated intensities) and X_{ij}^{calc} (extracted from the simulated intensities) with $X = P$ and $X = R$ was numerically estimated by computing a relative mean difference,

$$\epsilon = \left\langle \frac{|X_{ij}^{\text{theo}} - X_{ij}^{\text{calc}}|}{|X_{ij}^{\text{theo}}|} \right\rangle. \qquad [24]$$

The efficiency of the proposed method was evaluated on simulated noisy data, obtained by adding Gaussian noise. Also, the noise level was measured on each 2D experimental data set. In both cases, the noise level (expressed in percentages on the intensity) is estimated as

$$\sigma_{ij} = 100\, \frac{e_{ij}}{\langle |\mathcal{J}_{ij}(\theta, \tau_m)| \rangle_{ij}}, \qquad [25]$$

where e_{ij} is the error (thermal noise) measured on the set of experimental intensities or the standard deviation of the Gaussian noise added to simulated intensities, and $\langle |\mathcal{J}_{ij}(\theta, \tau_m)| \rangle_{ij}$ is the average absolute intensity of the (I^i, I^j) cross-peak, computed from the set of cross-peak intensities simulated or measured at each value of (θ, τ_m). The σ_{ij} values encountered for simulated intensities are always larger than 2% (resp., 4 and 8%) for e_{ij} values of 0.005 (resp., 0.001 and 0.002).

The method of cross-relaxation rate determination is implemented through macro commands using the program Tela 1.2 (*39*).

4.2. Acquisition

The peptide ranalexin was synthesized using a protocol described elsewhere (*33*). A water sample was prepared by dissolving 2.5 mg of peptide in 500 μl of water, to obtain a 2-mM sample, at pH 3.7. A trifluoroethanol sample of concentration 1.5 mM was prepared from the water sample by addition of 30% of TFE.

Experiments were recorded on a Bruker AMX spectrometer operating at 600 MHz at a temperature of 285 K in water and at a temperature of 290 K in TFE. Eleven off-resonance

ROESY experiments were recorded with the following values of the angle θ: 5, 10, 15, 20, 25, 30, 35, 40, 45, 50, and 55°. The RF irradiation was alternatively shifted up or down to the carrier frequency, in order to acquire quantitative off-resonance ROESY matrices (*22, 40*). A trapezoidal RF irradiation was used to allow adiabatic rotations of the magnetization (*20*) and thus to minimize the loss of spin magnetization by direct projection from the static to the effective field axis. In water, the variation of the angle θ was obtained by varying the offset Δ from 87.9 to 5.4 kHz, the RF irradiation amplitude being kept constant at 7.7 kHz. In TFE, the amplitude was 7.6 kHz, and the offset varied from 85.8 to 5.2 kHz. The spectral width in both dimensions was 7042 Hz. According to the experimental conditions used (offset Δ kept larger than $\frac{3}{4}$ of the proton spectral width), it was previously shown (*22*) that the angular dispersion induces at most a relative error on intensities of 3%; the associated distribution of the angle θ is less than 0.6°. The mixing time value was 200 ms. The water suppression in the off-resonance ROESY experiments was achieved by the WATERGATE sequence (*20, 41*). Thirty-two transients were acquired for each t_1 experiment, and 64 dummy transients were recorded at the beginning of each 2D experiment. The duration of each off-resonance ROESY experiment was about 7 h.

4.3. Spectral Processing

Processing and analysis of the data sets were performed by using the Gifa NMR processing program (*42*). The size in F1 was increased from 512 to 1024 points by zero-filling. The data sets were apodized by 18° shifted squared sine bells on both dimensions. After Fourier transformation, a polynomial baseline correction (*43*) was applied in both dimensions.

The $\theta = 5°$ experiment was used to determine a set of peaks by peak-picking of amide–amide, aliphatic–aliphatic, and amide(F1)–aliphatic(F2) regions. The peak-picking was then labeled using the ranalexin assignment (*33*) and the assignment module developed in Gifa (*44*) for computer-aided spectral assignment. Peak integration masks were determined on this experiment using a previously described method (*45*). Each peak volume was then computed by summing the intensities on the peak integration mask. The intensities of the thermal noise e_{ij} were derived from the mask size and the integration volume of the noise on the spectra.

ACKNOWLEDGMENTS

The authors thank Dr. Patrice Koehl and Dr. Patrick Berthault for fruitful discussions. CNRS, INSERM, and CEA are acknowledged for funding.

REFERENCES

1. A. T. Brünger and M. Nilges, Computational challenges for macromolecular structure determination by X-ray crystallography and solution NMR-spectroscopy, *Q. Rev. Biophys.* **26,** 49–125 (1993).
2. C. G. Hoogstraten and J. L. Markley, Effects of experimentally achievable improvements in the quality of NMR distance constraints on the accuracy of calculated protein structures, *J. Mol. Biol.* **258,** 334–348 (1996).
3. C. G. Hoogstraten, W. M. Westler, S. Macura, and J. L. Markley, Improved measurement of longer proton–proton distances in proteins by relaxation network editing, *J. Magn. Reson. B* **102,** 232–235 (1993).
4. C. Zwahlen, S. J. F. Vincent, L. Di Bari, M. H. Levitt, and G. Bodenhausen, Quenching spin diffusion in selective measurements of transient Overhauser effects in nuclear magnetic resonance. Applications to oligonucleotides, *J. Am. Chem. Soc.* **116,** 362–368 (1994).
5. B. A. Borgias and T. L. James, MARDIGRAS: A procedure for matrix analysis of relaxation for discerning geometry of an aqueous structure, *J. Magn. Reson.* **87,** 475–487 (1988).
6. R. Boelens, T. M. G. Koning, G. A. van der Marel, J. H. van Boom, and R. Kaptein, Iterative procedure for structure determination from proton–proton NOEs using a full relaxation matrix approach. Application to a DNA octamer, *J. Magn. Reson.* **82,** 290–308 (1989).
7. C. B. Post, R. P. Meadow, and D. G. Gorenstein, On the evaluation of interproton distances for three-dimensional structure determination by NMR using a relaxation rate matrix analysis, *J. Am. Chem. Soc.* **112,** 6796–6803 (1990).
8. M. Madrid, E. Llinas, and M. Llinas, Model-independent refinement of interproton distances generated from 1H NMR Overhauser intensities, *J. Magn. Reson.* **93,** 329–346 (1991).
9. P. Yip and D. A. Case, A new method for refinement of macromolecular structures based on nuclear Overhauser effect spectra, *J. Magn. Reson.* **83,** 643–648 (1989).
10. P. Koehl and J. F. Lefèvre, The reconstruction of the relaxation matrix from an incomplete set of NOEs, *J. Magn. Reson.* **86,** 565–583 (1990).
11. T. E. Malliavin, M. A. Delsuc, and J. Y. Lallemand, Computation of Redfield matrix element from incomplete NOESY data-sets, *J. Biomol. NMR* **2,** 349–360 (1992).
12. S. G. Hyberts and G. Wagner, Taylor transformation of 2D NMR τ_m series from time dimension to polynomial dimension, *J. Magn. Reson.* **81,** 418–422 (1989).
13. D. G. Davis, A novel method for determining internuclear distances and correlations times from NMR cross-relaxation rates, *J. Am. Chem. Soc.* **109,** 3471–3472 (1987).
14. B. T. Farmer II, S. Macura, and L. R. Brown, The effect of molecular motion on cross relaxation in the laboratory and rotating frames, *J. Magn. Reson.* **80,** 1–22 (1988).
15. H. Desvaux, P. Berthault, and N. Birlirakis, Dipolar spectral density from off-resonance ^{1}H NMR relaxation measurements, *Chem. Phys. Lett.* **233,** 545–549 (1995).
16. A. Bax and D. G. Davis, Practical aspects of two-dimensional transverse NOE spectroscopy, *J. Magn. Reson.* **63,** 207–213 (1985).
17. A. A. Bothner-By, R. L. Stevens, J. T. Lee, C. D. Warren, and R. W. Jeanloz, Structure determination of a tetrasaccharide: Transient nuclear Overhauser effects in the rotating frame, *J. Am. Chem. Soc.* **106,** 811–813 (1984).
18. J. Schleucher, J. Quant, S. J. Glaser, and C. Griesinger, A theorem relating cross-relaxation and Hartman–Hahn transfer in multiple-pulse sequences. Optimal suppression of TOCSY transfer in ROESY, *J. Magn. Reson. A* **112,** 144–151 (1995).
19. H. Desvaux, P. Berthault, N. Birlirakis, and M. Goldman, Off-resonance ROESY for the study of dynamic processes, *J. Magn. Reson. A* **108,** 219–229 (1994).

20. H. Desvaux, P. Berthault, N. Birlirakis, M. Goldman, and M. Piotto, Improved versions of off-resonance ROESY, *J. Magn. Reson. A* **113,** 47–52 (1995).

21. K. Kuwata and T. Schleich, Polarization-operator formalism description of the off-resonance ROESY experiment, *J. Magn. Reson. A* **114,** 219–229 (1995).

22. T. E. Malliavin, H. Desvaux, and M. A. Delsuc, Conditions for the measurement of quantitative off-resonance ROESY intensities, *Magn. Reson. Chem.* **36,** 801–806 (1998).

23. P. Berthault, N. Birlirakis, G. Rubinstenn, P. Sinaÿ, and H. Desvaux, Solution structure of a Lewis^{x} analogue by off-resonance ^{1}H NMR spectroscopy without use of an internal distance reference, *J. Biomol. NMR* **8,** 23–35 (1996).

24. M. Guenneugues, P. Drevet, S. Pinkasfeld, B. Gilquin, A. Menez, and S. Zinn-Justin, Picosecond to hour time scale dynamics of a "three finger" toxin: Correlation with its toxic and antigenic properties, *Biochemistry* **36,** 16097–16108 (1997).

25. V. Dive, P. Cuniasse, I. Raynal, and A. Yiotakis, Accounting for conformational variability in NMR structure of cyclopeptides: Ensemble averaging of interproton distance and coupling constant restraints, *J. Am. Chem. Soc.* **119,** 5239–5248 (1997).

26. K. Kuwata, H. Liu, T. Schleich, and T. L. James, Rotational correlation times of internuclear vectors in a DNA duplex with A–G mismatch determined in aqueous solution by complete relaxation matrix analysis of off-resonance ROESY (O-ROESY) spectra, *J. Magn. Reson.* **128,** 70–81 (1997).

27. H. Desvaux and P. Berthault, Study of dynamic processes in liquids using off-resonance rf irradiation, *Prog. NMR Spectrosc.,* in press (1999).

28. I. Solomon, Relaxation processes in a system of two spins, *Phys. Rev.* **99,** 559–565 (1955).

29. J. D. Baleja and B. D. Sykes, Correlation time adjustment factors for NOE-based structure refinement, *J. Magn. Reson.* **91,** 624–629 (1991).

30. J. W. Keepers and T. L. James, A theoretical study of distance determination from NMR 2D NOE spectra, *J. Magn. Reson.* **57,** 404–426 (1984).

31. S. Macura and R. R. Ernst, Elucidation of cross relaxation in liquids by two dimensional NMR spectroscopy, *Mol. Phys.* **41,** 95–117 (1980).

32. Y. Liu, D. Zhao, R. Altman, and O. Jardetzky, A systematic comparison of three structure determination methods from NMR data: Dependence upon quality and quantity of data, *J. Biomol. NMR* **2,** 373–388 (1992).

33. E. Vignal, A. Chavanieu, P. Roch, L. Chiche, G. Grassy, B. Calas, and A. Aumelas, Solution structure of the antimicrobial peptide ranalexin and a study of its interaction with perdeuterated dodecylphosphocholine micelles, *Eur. J. Biochem.* **253,** 221–228 (1998).

34. D. S. Wishart and B. D. Sykes, The ^{13}C chemical-shift index: A simple method for the identification of protein secondary structure using ^{13}C chemical-shift data, *J. Biomol. NMR* **4,** 171–180 (1994).

35. T. E. Malliavin, M. A. Delsuc, V. Y. Orekhov, and A. S. Arseniev, An estimate of spin diffusion in a spin subset: Application to iterative distance calculation from 3D N-15 NOESY-HMQC, *J. Biomol. NMR* **5,** 193–201 (1995).

36. B. Gilquin, C. Roumestand, S. Zinn-Justin, A. Menez, and F. Toma, Refined 3-dimensional solution structure of a snake cardiotoxin—Analysis of the side-chain organization suggests the existence of a possible phospholipid binding site, *Biopolymers* **33,** 1659–1675 (1993).

37. A. G. Palmer, R. A. Hochstrasser, D. P. Millar, M. Rance, and P. E. Wright, Characterization of amino acid side chain dynamics in a zinc-finger peptide using C-13 NMR spectroscopy and time-resolved fluorescence spectroscopy, *J. Am. Chem. Soc.* **115,** 6333–6345 (1993).

38. M. Buck, J. Boyd, C. Redfield, D. A. Mackenzie, D. J. Jeenes, D. B. Archer, and C. M. Dobson, Structural determinants of protein dynamics: Analysis of N-15 NMR relaxation measurements for main-chain and side-chain nuclei of hen egg white lysozyme, *Biochemistry* **34,** 4041–4055 (1995).

39. P. Janhunen, Tela 1.2, http://www.geo.fmi.fi/prog/tela.html (1993).

40. H. Desvaux and M. Goldman, A simple solution to decrease angular dispersion in off-resonance experiments, *J. Magn. Reson B* **110,** 198–201 (1996).

41. V. Sklenar, M. Piotto, R. Leppik, and V. Saudek, Gradient-tailored water suppression for H-1–N-15 HSQC experiments optimized to retain full sensitivity, *J. Magn. Reson. A* **102,** 241–245 (1993).

42. J. L. Pons, T. E. Malliavin, and M. A. Delsuc, Gifa V4: A complete package for NMR data set processing, *J. Biomol. NMR* **8,** 445–452 (1996).

43. A. Rouh, M. A. Delsuc, G. Bertrand, and J. Y. Lallemand, Baseline correction of FT NMR spectra: An approach in terms of classification, *J. Magn. Reson. A* **102,** 357–359 (1993).

44. T. E. Malliavin, J. L. Pons, and M. A. Delsuc, An NMR assignment module implemented in the GIFA NMR processing program, *Bioinformatics* **14,** 624–631 (1998).

45. V. Stoven, A. Mikou, D. Piveteau, E. Guittet, and J. Y. Lallemand, Paris, a program for automatic recognition and integration of 2D NMR signals, *J. Magn. Reson.* **82,** 163–168 (1989).